Available online at www.sciencedirect.com
SCIENCE DIRECT®
Physica B 351 (2004) 213–226
PHYSICA B
www.elsevier.com/locate/physb

Simulation of ballistic and non-Fourier thermal transport in ultra-fast laser heating

Jun Xu, Xinwei Wang*

Department of Mechanical Engineering, N104 Walter Scott Engineering Center, The University of Nebraska-Lincoln, Lincoln, NE 68588-0656, USA

Received 2 March 2004; accepted 4 June 2004

Abstract

In this work, the lattice Boltzmann method (LBM) is developed to simulate pico- and femtosecond laser heating of silicon. The temperature fields calculated by the LBM are compared with those obtained from the parabolic heat conduction equation (PHCE) and the hyperbolic heat conduction equation (HHCE). Although the HHCE overcomes the dilemma of infinite thermal propagation speed of the PHCE, it cannot be applied to length scales comparable to the mean free path of energy carriers because of the breakdown of continuum approaches under severe nonequilibrium conditions. The LBM, considering both effects, can be used in both short temporal and spatial scales. From the results of the LBM, it is found that the speed of thermal wave at the ballistic limit is equal to the speed of sound, instead of the value predicted by the HHCE, which is valid only in the diffuse limit. It is also demonstrated that the traditional way of calculating heat flux using the temperature gradient gives rise to physically unreasonable results at the thermal wave front, while the LBM has no such drawback.

PACS: 44.10.+i; 44.90.+c; 67.40.Pm

Keywords: Phonons; Laser heating; Ballistic transport; Non-Fourier transport; Thermal wave

1. Introduction

Although the parabolic heat conduction equation (PHCE), which is based on the Fourier's law, agrees well with experiment for conventional heat transfer problems, it is known to be invalid in thermal transport at very short time scales (pico- and femtoseconds) due to its physically unreasonable assumption of infinite speed of thermal propagation. The hyperbolic heat conduction equation (HHCE), assuming a certain time lag for heat flux behind the temperature gradient, has been extensively used to investigate non-Fourier thermal transport [1,2]. The solutions to the HHCE show that energy disturbances travel as damped waves, and the predicted temperature and

*Corresponding author. Tel.: +1-402-472-3089; fax: +1-402-472-1465.
E-mail address: xwang3@unl.edu (X. Wang).

0921-4526/$ - see front matter © 2004 Elsevier B.V. All rights reserved.
doi:10.1016/j.physb.2004.06.009

Nomenclature

$\vec{c}$	nondimensionalized phonon velocity
c_p	specific heat per unit mass
$D(\omega)$	density of states
e	energy distribution function
E	nondimensionalized energy distribution function
$\vec{F}$	external force
f	distribution function of particles
$\hbar$	Plank's constant divided by 2π
I	intensity of the laser beam
k	thermal conductivity
l	phonon mean free path in bulk materials
L	film thickness
L_0	lattice length used in the Lattice Boltzmann Method
$\vec{n}$	unit vector
$\vec{p}$	momentum
$\vec{q}''$	heat flux
$\dot{Q}$	rate of energy generation
$\vec{r}$	position
R	nonequilibrium characterization parameter
s	source term induced by laser heating
S	nondimensionalized source term
t	time
t_0	time of the peak intensity of the laser pulse
t_g	characteristic parameter of the Gaussian function
T	temperature
u	energy density
$\vec{v}$	speed of sound
$\vec{v}_T$	speed of thermal wave
z	coordinate normal to a film

Greek Symbols

α	thermal diffusivity
β	optical absorption coefficient
ρ	mass density
τ	relaxation time
ω	angular frequency of phonons

Superscripts

0	equilibrium
$*$	nondimensionalized

Subscripts

i,j	indices of the direction

heat flux are much different from those of the PHCE when the elapsed time is comparable to the mean free time of energy carriers. This equation, however, is questionable under circumstances with strong nonequilibrium characteristics because of its physical defects. Bai and Lavine [3] pointed out that the HHCE may not obey the second law of thermodynamics. In order to remedy this drawback, they solved a modified hyperbolic heat conduction equation, which takes into account the nonequilibrium effect. Körner and Bergmann [4] showed that the HHCE violates the conservation of energy due to its neglect of the spatial nonlocality of thermal transport. Both Refs. [3,4] demonstrated that the HHCE led to negative absolute temperatures under certain conditions, which is physically unreasonable. Furthermore, the HHCE does not differ much from traditional approaches in that it is still based on the continuum hypothesis, which breaks down in very small spatial domains. Majumdar [5] proved that the HHCE is just an approximation of the more fundamental Boltzmann transport equation (BTE) under equilibrium assumption and is not suitable for microscale regime. From the BTE, Chen [6] developed the ballistic-diffusive heat-conduction equations and demonstrated that the HHCE corresponds only to the diffusive part of his model. Therefore, it is desirable to adopt methods directly based on the microscopic view of transport to deal with problems involving both small temporal and spatial scales. To date, there has been a trend of using discrete models to study thermal transport at micro/nanoacales. Recently, Xu [7] used the lattice Boltzmann method (LBM), a numerical scheme for solving the BTE, to examine thin film heat conduction in dielectric materials and found that the ballistic transport near boundaries can make temperature and heat flux deviate significantly from the prediction of the

Fourier's law. In that study, however, time scale is not discussed in detail. Since the LBM is derived from the basic transport equation and implemented with a discrete formulation compatible with microscopic perspectives, it is able to obtain physically reasonable results.

In this work, the LBM is used to study the thermal transport phenomena in very short time and length domains in ultra-fast laser heating of materials. In this process, the energy is absorbed within a few optical absorption depths beneath the irradiated surface within a duration of femtoseconds (fs: 10^{-15} s) or picoseconds (ps: 10^{-12} s). The transport of thermal energy is accompanied with a very high heat flux and temperature-changing rate and is usually limited to very small domains at early stages. In this work, the LBM is used to study the temperature evolution in a silicon slab exposed to laser pulses with a Gaussian distribution in the time domain. The results are compared with those of the HHCE and PHCE.

2. Fundamentals

Traditionally, heat conduction problems with internal heat sources are solved using the parabolic heat conduction equation (PHCE) [8]

$$\frac{1}{\alpha}\frac{\partial T}{\partial t} = \nabla^2 T + \frac{\dot{Q}}{k} \tag{1}$$

where T is temperature, t is time, α and k are thermal diffusivity and thermal conductivity, and $\dot{Q}$ is the rate of energy generation (W/m^3).

One flaw of the PHCE is that it allows a thermal disturbance to be instantly sensed anywhere in the medium regardless of the distance. This is physically unreasonable because energy carriers need time to move and collide. A modification to the Fourier's law assumes a buildup time for heat flux following an established temperature gradient. It is proposed as [9]

$$\vec{q}''(t+\tau) = -k\nabla T, \tag{2}$$

where τ is called the thermal relaxation time and is usually calculated with equations of the kinetic theory, $k = \rho c_p v l/3$ and $\tau = l/v$, where ρ is mass density, c_p is specific heat, v is the speed of sound and l is the mean free path (MFP). Roughly, τ can be regarded as the average time an energy carrier travels between successive collisions.

The first-order truncation of the left-hand side of Eq. (2) is inserted into the conservation equation

$$\rho c_p \frac{\partial T}{\partial t} = -\nabla \cdot \vec{q}'' + \dot{Q} \tag{3}$$

which leads to the hyperbolic heat conduction equation (HHCE)

$$\frac{\tau}{\alpha}\frac{\partial^2 T}{\partial t^2} + \frac{1}{\alpha}\frac{\partial T}{\partial t} = \nabla^2 T + \frac{1}{k}\left(\dot{Q} + \tau\frac{\partial \dot{Q}}{\partial t}\right). \tag{4}$$

Eq. (4) implies that a heat pulse travels as a wave attenuated by diffusion.

Although the HHCE provides a great advance in comparison with the PHCE, it is still based on macroscopic concepts, which assume that thermal equilibrium is always established locally. This may not hold true for situations with strong nonequilibrium energy distributions, which are commonly found in extreme small domains. Derived from the statistical theory of particles, the Boltzmann transport equation (BTE) is becoming popular in studies of thermal transport because it is not limited to continuum models. In dielectric materials and semiconductors, phonons are the dominant energy carriers and the transport by electrons can be neglected. The basic form of the phonon BTE is [10]

$$\frac{\partial f}{\partial t} + \vec{v}\cdot\nabla f + \vec{F}\cdot\frac{\partial f}{\partial \vec{p}} = \left(\frac{\partial f}{\partial t}\right)_{\text{scatt}}, \tag{5}$$

where f is the distribution of phonons as a function of position $\vec{r}$, time t, frequency ω and velocity $\vec{v}$. In this study, the external force $\vec{F}$ is omitted since it has negligible effect on thermal transport. The remaining terms on the left-hand side of Eq. (5) represent the streaming of phonons with their own velocities. The right-hand side of Eq. (5) deals with all scattering factors, including phonon–phonon, phonon–defect and phonon–electron collisions. The collision leading to energy transfer from light to heat is assumed to be much faster than the phonon thermal transport. Hence,

the laser absorption can be approximated as a heating source as if the laser energy is absorbed immediately while passing through the media. At the same time, the remainder of the collision term, which is directly responsible for energy transport, is simplified by the single relaxation-time approximation provided that the temperature rise is within a small range [11]. Hence, Eq. (5) is modified as

$$\frac{\partial f}{\partial t}+\vec{v}\cdot\nabla f=-\frac{f-f^0}{\tau}+\left(\frac{\partial f}{\partial t}\right)_{\text{laser heating}}, \tag{6}$$

where f^0 is the expected equilibrium distribution and τ is the relaxation time of phonons, which is identical to the one in Eq. (4). Note that τ is a function of phonon frequency. In our treatment, an average value for τ simplifies the computation but still enables the essential physics to be captured. Compared with the HHCE, the BTE considers not only the wave-like behavior of thermal processes, but also the variation of particle distribution in different propagation directions, which is necessary for predicting the ballistic transport.

3. Formulation of the LBM in laser heating problems

To further simplify the problem, the phonon velocity $\vec{v}$ in Eq. (6) is assumed to have a constant magnitude equal to the speed of sound, as in the Debye model, so that f can be written as $f(\omega,\vec{n},\vec{r},t)$, where $\vec{n}$ is the unit vector designating the propagating direction. Considering that phonons have different polarizations, the energy distribution function is obtained as the following summation over integrations;

$$e(\vec{n},\vec{r},t)=\sum_{\mathrm{p}}\int\hbar\omega f_{\mathrm{p}}(\omega,\vec{n},\vec{r},t)D(\omega)\,\mathrm{d}\omega, \tag{7}$$

where subscript p stands for a particular polarization and $D(\omega)$ is the density of states. Applying Eq. (7) to each term in Eq. (6) yields the equation directly related to the energy distribution,

$$\frac{\partial e}{\partial t}+\vec{v}\cdot\nabla e=-\frac{e-e^0}{\tau}+s, \tag{8}$$

where the source term s, which is the integration containing $(\partial f/\partial t)_{\text{laser heating}}$, represents the energy increase attributed to laser heating.

To solve Eq. (8) by the LBM, discretization is carried out using a cubic lattice pattern shown in Fig. 1. The energy distribution at any node is assigned to six components, $e_i(\vec{r},t)$, where $i=1,2,\ldots,6$, representing the six outward directions along Cartesian coordinates. Thus, Eq. (8) yields six component equations

$$\frac{\partial e_i}{\partial t}+\vec{v}_i\cdot\nabla e_i=-\frac{e_i-e_i^0}{\tau}+s_i. \tag{9}$$

To discretize the differential operation, the space step is chosen to equal the lattice length $|\Delta\vec{r}_i|=L_0$ and the time step is set to satisfy $\Delta t=L_0/|v_i|$. Thus, Eq. (9) is discretized in the form

$$\begin{aligned}&e_i(\vec{r}+\Delta\vec{r}_i,t+\Delta t)-e_i(\vec{r},t)\\&=-\frac{e_i(\vec{r},t)-e_i^0(\vec{r},t)}{\tau^*}+s_i\cdot\Delta t,\end{aligned} \tag{10}$$

where $\tau^*=\tau/\Delta t$.

The energy density at a node is the sum of e_i's over all the directions,

$$u=\sum_{i=1}^{6}e_i. \tag{11}$$

The expected equilibrium distribution is given by averaging the above values

$$e_i^0=\frac{1}{6}\sum_{i=1}^{6}e_i. \tag{12}$$

Intially, the whole system is in equilibrium so that $e_i(\vec{r},t=0)=e_i^0(\vec{r},t=0)$.

The net heat flux in the x, y and z directions can be, respectively, obtained as

$$q_j''=v(e_j^+-e_j^-), \tag{13}$$

where the subscript j can be x, y or z. e^+ and e^- represent the heat fluxes in the positive and negative directions, respectively.

The energy density is related to temperature by

$$u=\int_0^T\rho c_p\;d\xi. \tag{14}$$

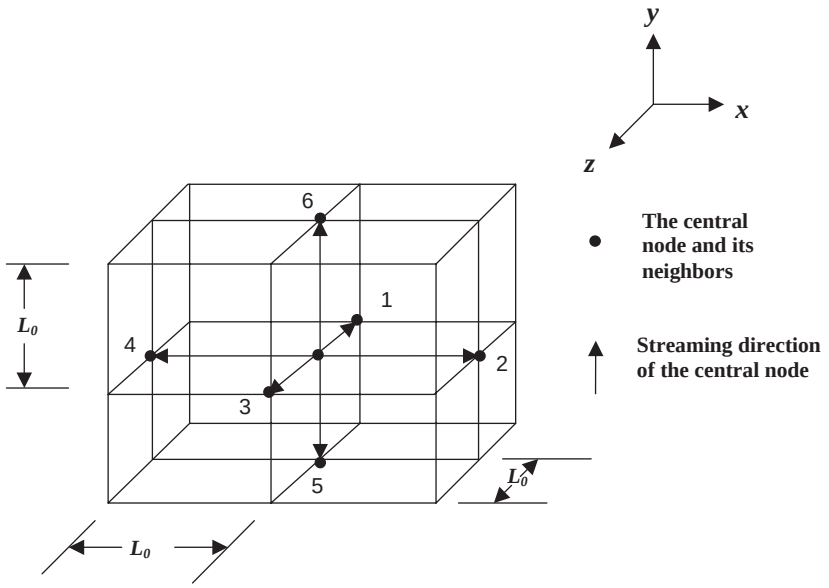

Fig. 1. Schematic of a three-dimensional lattice.

For convenience, the temperature increase is calculated by

$$\Delta T = \frac{\Delta u}{\rho c_p} \tag{15}$$

provided that ΔT is moderate so that there is no phase change and the specific heat can be regarded as a constant.

In the model problems, one surface of a silicon sample is exposed to a spatially uniform laser pulse with a Gaussian distribution in the time domain as shown in Fig. 2,

$$I = I_0 \exp\left[-\left(\frac{t - t_0}{t_g}\right)^2\right], \tag{16}$$

where I_0 is the peak power intensity, t_0 and t_g are characteristic parameters of the Gaussian distribution.

The absorption of laser radiation is assumed to obey the Beer's law, i.e., the volumetric heat generation rate at depth x is

$$\dot{Q} = \beta I \exp(-\beta x)$$

$$= \beta \cdot I_0 \exp(-\beta x) \exp\left[-\left(\frac{t - t_0}{t_g}\right)^2\right], \tag{17}$$

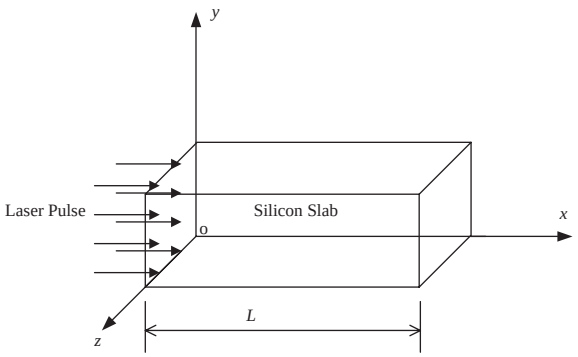

Fig. 2. Schematic of the laser heating model.

where β is the coefficient of optical absorption. This amount of energy should be allocated equally to all directions, hence

$$s_i = \frac{1}{6}\dot{Q} = \frac{1}{6}\beta I_0 \exp(-\beta x) \exp\left[-\left(\frac{t - t_0}{t_g}\right)^2\right],$$

$$i = 1, 2, \ldots, 6. \tag{18}$$

Since obtaining the absolute value of the internal energy is almost impossible and unnecessary,

Eq. (10) is nondimensionalized as

$$E_i(\vec{r}^* + \vec{c}_i, t^* + 1) - E_i(\vec{r}^*, t^*) = -\frac{E_i(\vec{r}^*, t^*) - E_i^0(\vec{r}^*, t^*)}{\tau^*} + S_i, \quad (19)$$

where $\vec{r}^* = \vec{r}/L_0$, $\vec{c}_i = \vec{v}_i/|\vec{v}_i|$, $t^* = vt/L_0$, $E_i = \left[e_i - e_i^0(t=0)\right]/(\beta I_0 \cdot \Delta t)$, $S_i = s_i/(\beta I_0)$. Here, E_i is a measure of the internal energy increase with respect to the initial condition, in which the entire system is at room temperature. For detailed algorithm of the LBM, readers can refer to recent publications [7,12].

Strictly speaking, different phonon branches (transverse, longitudinal, optical, acoustic) possess different group velocities and the use of a single speed of sound is just a rough estimate. However, as the first step to solve laser heating problems using the LBM, such simplification suffices to capture the essential physics. For more rigorous considerations, the LBM can be solved separately for different phonon branches and the combined energy distribution will give the total temperature and heat flux.

4. Results and discussion

Eq. (19) is solved for a model problem in which a laser pulse at wavelength 266 nm is incident on a silicon target (as shown in Fig. 2), which is initially at a uniform temperature of 300 K. The duration of the laser pulse ranges from nanoseconds (ns: 10^{-9} s) down to femtosecond in three computational cases. The laser beam is evenly distributed over the surface so that the temperature variation only exists in the x direction. On the back and front surfaces, adiabatic boundary conditions are employed. To simulate a domain with an infinite surface area, periodic boundary conditions are applied to the boundaries in the y and z directions. For comparison, the results obtained from the PHCE and HHCE are also presented. To solve the PHCE, the fully implicit scheme of the finite different method was used [13]. To solve the HHCE, the laser pulse is first treated as one cycle of a periodically fired laser beam whose period is much longer than the pulse duration. The heating source term in Eq. (4) is expanded into Fourier series. Each component of the Fourier series results in a particular solution and the final solution can be obtained by summing up all the particular ones because of the linearity of the equation. Details of this method can be found in the work by Wang and Xu [14]. The physical properties of silicon used in the simulation are listed in Table 1 [7]. The length of the x coordinate in the figures discussed below is tailored so that only the region with observable temperature rise is displayed.

It should be noted that the laser heating described in this problem is one-dimensional and hence the energy propagation occurs only in the longitudinal direction. The use of orthogonal lattice in heat conduction problems is validated by Wolf-Gladrow [15]. In laser heating problem involving three-dimensional heat conduction, higher order formulations with non-orthogonal lattice structure accounting for three-dimensional energy propagation might be more appropriate. Recently, Murthy and Mathur used unstructured polyhedric domains to discretize the BTE for solving sub-micron thermal transport problems [16]. They also combined a ray-tracing technique with the finite volume method to substantially improve the predictive accuracy of the finite volume method [17]. Similar methods may be developed to improve the accuracy of the LBM for more complicated applications.

Table 1
Physical properties of silicon used in the calculation

Specific heat c_p (J/kg K)	Mass density ρ (kg/m^3)	Thermal conductivity k (W/m K)	Phonon velocity v (m/s)	Mean free path l (nm)	Coefficient of optical absorption β (m^{-1})	Mean free time τ (ps)
712	2330	148	6509.78	41.1	2.10×10^8	6.32

4.1. Temperature evolution in the target irradiated by a nanosecond laser

As a verification of our model, the LBM is first used for a situation without strong non-Fourier effect. The laser pulse has an intensity described by Eq. (16) with $t_0 = 10$ and $t_g = 3$ ns. The fluence of the pulse is 60 J/m^2. This energy is chosen to make the temperature increase moderate so that the assumption of constant specific heat holds true. The laser fluences in the following cases also comply with this restriction. The temperature profiles are calculated with the LBM, HHCE and PHCE at 4 instants. Fig. 3 shows that the results from all these three methods are close to each other. The full-width at half-maximum (FWHM) of this laser pulse is 5 ns, which is much longer than the phonon mean free time 6.32 ps. The domain is 4 μm long, nearly 100 times the mean free path. This case can be regarded as temporally and spatially macroscopic, therefore both the HHCE and the LBM are equivalent to the PHCE. The sound agreement between the results of the LBM and the PHCE in this case demonstrates the validity of the LBM for solving heat transfer problems in laser-material interaction.

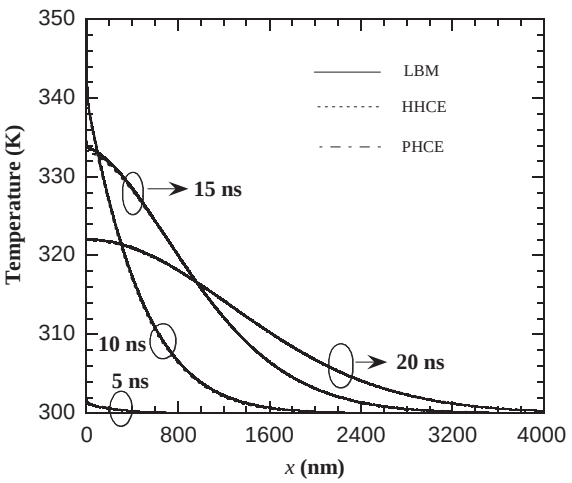

Fig. 3. Temperature distributions along the x direction in the target for nanosecond laser heating.

4.2. Temperature evolution in the target irradiated by a picosecond laser

The duration of the laser pulse is reduced with $t_0 = 10$ and $t_g = 3$ ps. The fluence of the laser pulse is 0.7 J/m^2. Fig. 4a–c show the temperature profiles along the x direction in the target at four instants. At 10 ps, all methods give temperatures decreasing continuously from the surface to the interior as expected. However, both the HHCE and the LBM predict higher temperature rises near the front surface and lower temperature rises inside than the PHCE does. This is because, in the first two models, the thermal wave propagates at a finite speed and the energy absorbed at the surface cannot be dissipated so quickly into the inner part of the material. In comparison with the HHCE, the LBM predicts a steeper temperature profile, which is typical of ballistic transport [5]. From Fig. 4a it is evident that the thermally affected domain at 10 ps is less than 60 nm, which is in the same order of the phonon MFP for silicon (41.1 nm), the collisions between phonons are actually scarce, resulting in weak diffusion of energy. On the other hand, the transport by direct streaming of phonons or ballistic transport is significant in this situation. The retarded transport brings about a tendency for the media to remain at the heated energy level. This phenomenon is similar to the temperature jumps at thin film boundaries predicted in previous studies [5,7]. Though the HHCE takes into account the finite speed of thermal transport, it fails to predict the ballistic aspect, which is important at sub-continuum scales.

At 30 ps, the temperature profile predicted by the PHCE levels off due to thermal diffusion. The solution to the HHCE is close to that of the PHCE near the front surface, while considerable deviation occurs at about $x = 70$ nm, where a hump appears in the temperature profile, corresponding to the front of the thermal wave. As for the result of the LBM, it can be divided into two parts: sharp dropping within 20 nm adjacent the boundary and gradual attenuation inside. The sudden temperature drop at the surface indicates that the ballistic transport plays an important role near the boundary. The wave front of thermal transport is

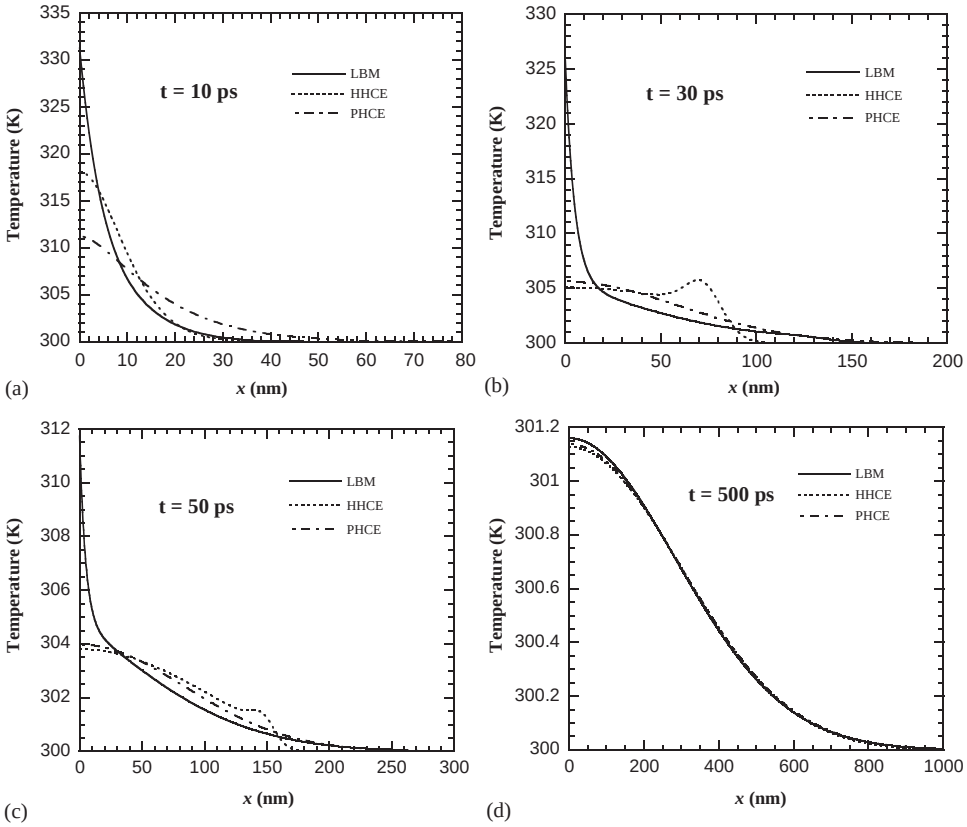

Fig. 4. Temperature distributions along the x direction in the target for picosecond laser heating.

not observed in the results by the LBM in this case. It is because a large proportion of the energy is concentrated in the near-surface region and the wave front is simply smoothed out. The results at 50 ps are similar to those at 30 ps. It can be seen that the temperature hump predicted by the HHCE has moved to $x = 150$ nm due to the inward propagation of the thermal wave. There is an appreciable difference in the boundary region, where the temperature rise predicted by the LBM is about two times higher than those by the other two.

At 500 ps, the temperature profiles predicted by both the LBM and the HHCE agree well with the solution of the PHCE. This is because thermal equilibrium has been well established within the material so that the non-Fourier and ballistic effects are now negligible. It can be seen in Fig. 4d that the thermal wave has traveled more than one micrometer and is completely damped by diffusion. Moreover, the temperature jumps in the near-surface region predicted by the LBM at earlier times no longer exist. These results confirm that the LBM and the HHCE are equivalent to the PHCE in the macroscopic limit.

To have a better view of the nonequilibrium characteristics of the system, the following parameter is defined:

$$R_i = \left(\frac{6e_i}{\rho c_p} - \frac{6e_i^0}{\rho c_p}\right)/T \tag{20}$$

in which $6e_i/\rho c_p$ represents an equivalent temperature associated with the energy in direction i, and $6e_i^0/\rho c_p$ is the corresponding equilibrium temperature. The stronger the nonequilibrium of the system, the larger will be the absolute value of R_i. The distribution of R's are plotted in Fig. 5. Subscript 2 represents the component in the laser

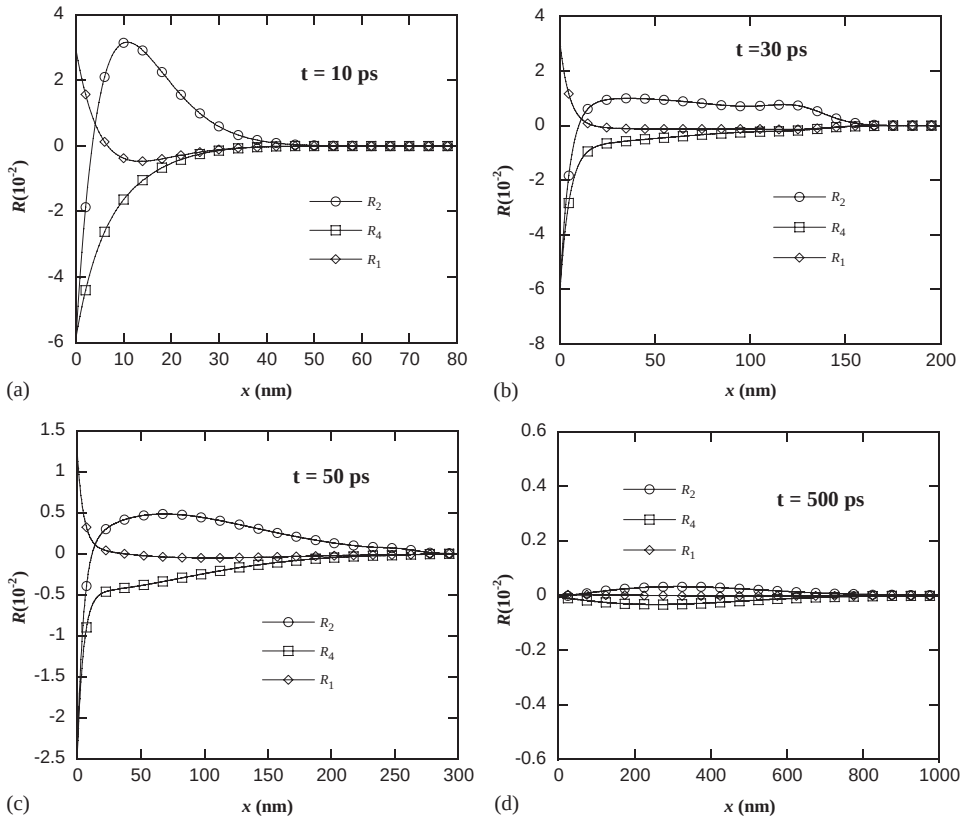

Fig. 5. Distribution of R's in the target for picosecond laser heating.

incidence direction. R_4 is opposite to R_2, and R_1 is associated with the energy flowing in one of the lateral directions (see Figs. 1 and 2). R_1, R_3, R_5, R_6 are identical attributed to the one-dimensional heating in our work, therefore only R_1 is plotted in Fig. 5. In diffusive thermal transport, the system is in quasi-equilibrium and each component e_i is equal to its equilibrium value so that the three curves should be all close to zero, i.e., $R_i \approx 0$. In ballistic transport, scattering is inadequate to provide uniformization of energies among different directions, leading to a non-uniform distribution. It can be seen from Fig. 5a–c that energy distributions are strongly unbalanced near the heated surface. This shows that energy is flowing ballistically rather than diffusively in the near-boundary region. Since both the PHCE and HHCE are based on the equilibrium hypothesis, which is invalid for these situations, it is expected that their results are remarkably different from the LBM's. However, as time increases, R_i's are gradually approaching zero, indicating that the system has a tendency to restore equilibrium. When $t = 500$ ps, the three curves are roughly zero, in agreement with the fact that microscopic and continuum models give similar temperature profiles at this moment (Fig. 5d). Another interesting feature in these plots is that the R_2 curve has a peak, which keeps moving inward and is flattened as it propagates. It is estimated that this region is shifting at the speed of sound. This indicates that the LBM has the capability to reveal wavelike thermal transport.

4.3. Temperature evolution in the target irradiated by a femtosecond laser

In Section 4.2, the FWHM of the laser pulse is 5 ps, which is of the same order of the mean free time of phonons (6.32 ps). In this section, a laser

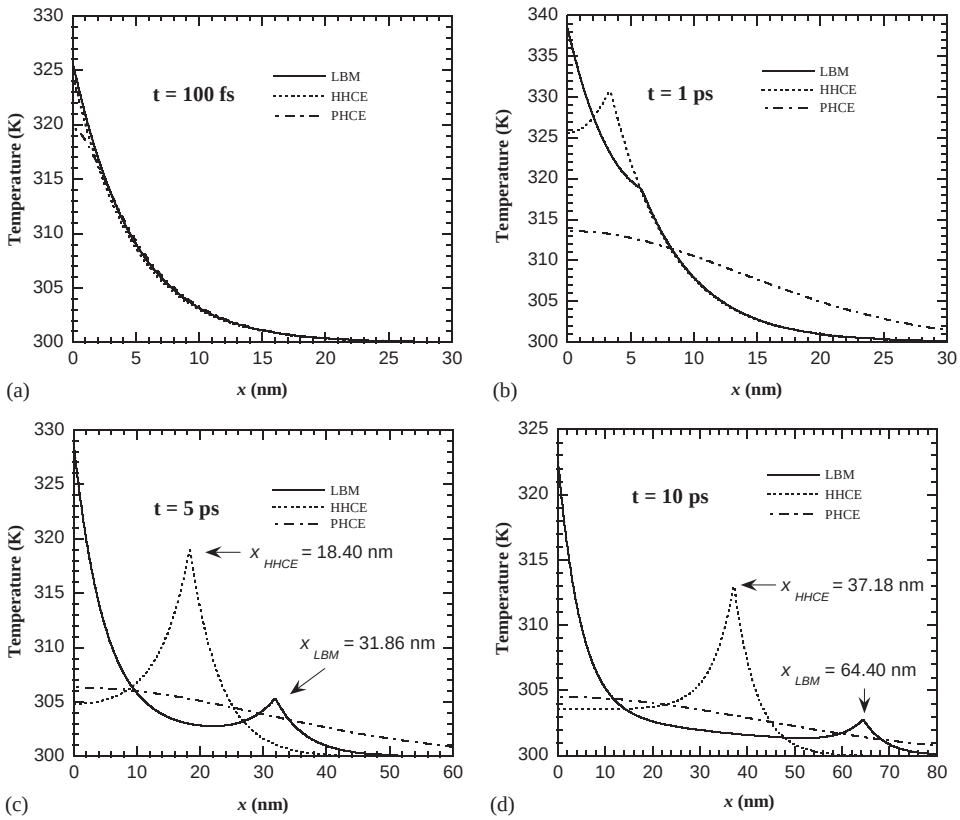

Fig. 6. Temperature distributions along the x direction in the target for femtosecond laser heating.

pulse with a Gaussian temporal distribution in which $t_0 = 100\,\text{fs}$ and $t_g = 30\,\text{fs}$ is applied to the same silicon target. The laser fluence takes $0.4\,\text{J/m}^2$. The corresponding FWHM is 50 fs, much shorter than the mean free time of phonons.

Fig. 6a–d present the temperature profiles at different times. The temperature profiles at 100 fs are shown in Fig. 6a. At this moment, the laser is still heating the target at a very high rate while there have not been enough interactions between phonons to conduct the thermal energy away. Therefore, the temperature change up to this point is dominated by the absorption of the laser energy rather than by thermal transport. In all the three methods, the heat source term is derived from the Beer's law, so it is not surprising that their results agree well with each other in most part of the domain except the near-surface region where the LBM and the HHCE predict higher temperature rises attributed to the retardation of thermal propagation. The laser absorption is assumed to be isotropic, which leads to equal increase of energy distribution in all directions. Since the wave effect plays a major role in this situation, the LBM and HHCE give close results for the temperature increase.

Fig. 6b shows the temperature profiles at 1 ps. At this instant, there is no longer direct heating from the laser and the temperature distribution is dominated by thermal transport. However, since t is still much smaller than the thermal relaxation time τ, the onset of heat flux is far behind the temperature gradient. Therefore, the temperature profiles predicted by the LBM and the HHCE differ strongly from that of the PHCE, illustrating that energy transfer from the hot region to the cold region is delayed. Although the results of the LBM and the HHCE match each other closely in the

inner region, they deviate much in the proximity of the front surface. It needs to be pointed out that both curves illustrate the presence of thermal waves, while they are at different locations. This demonstrates that thermal waves are not propagating at the same speed in the two models (discussed later). Furthermore, it can be seen in the result of the HHCE that the temperature increases with depth between the surface and the wave peak, in contrary to the expectation that temperature should be the highest at the heated surface. This temperature overshooting predicted by the HHCE was also reported in Refs. [3,4]. According to the work by Bai and Lavine [18], the physically unreasonable temperature field obtained from the HHCE can be remedied by using a continuum approach in the interior region in conjunction with jump thermal boundary conditions at the surface. In the result of the LBM, the surface temperature is always higher than interior temperature because of the presence of a boundary temperature jump associated with the ballistic effect.

In Fig. 6c and d, both the LBM and the HHCE demonstrate wave behavior with the temperature peaks moving in the thermal propagation direction. The apparent difference is that the temperature is lower at the surface than that at the wave front in the HHCE result, while it is always the highest at the surface in the LBM result. It is also observed that the wave front predicted by the LBM is much weaker than that of the HHCE. This can be explained by the fact that the boundary region accommodates much more energy in the LBM, leaving less energy available for the formation of thermal waves due to the conservation of energy in the system.

The R's in directions 1, 2, 4 are also plotted out for this case (Fig. 7a–d). It can be seen that at $t = 100$ fs the nonequilibrium is not strong due to

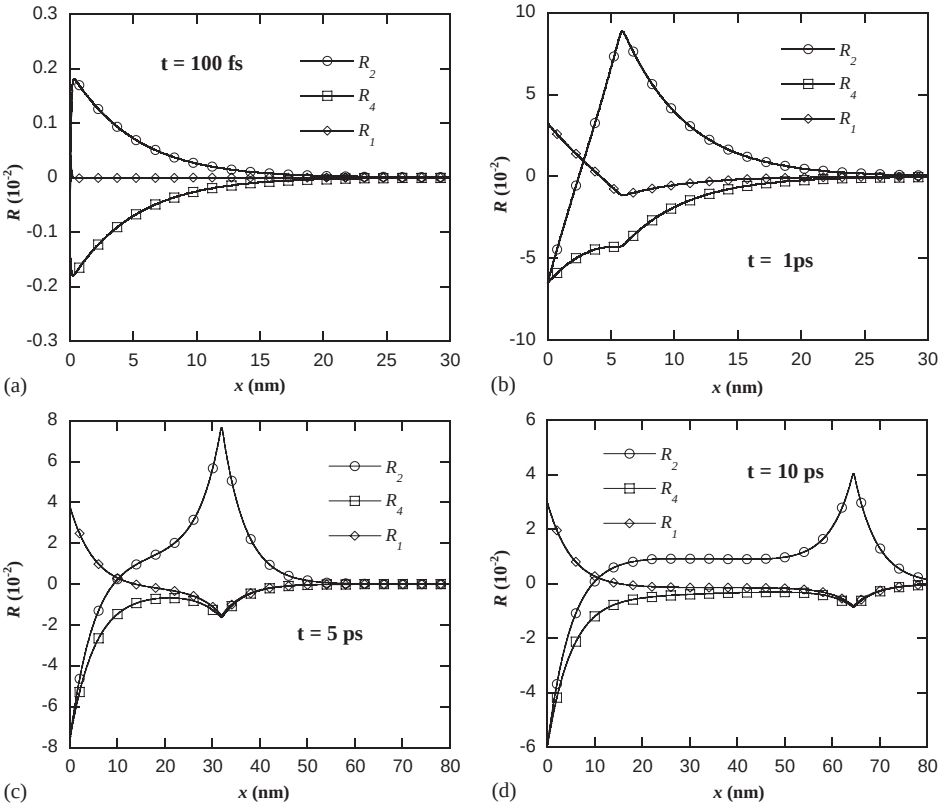

Fig. 7. Distribution of R's in the target for femtosecond laser heating.

the isotropic laser absorption. After the laser heating stops, thermal energy continues streaming to the inside region of the target, leading to gradual destruction of the original equilibrium, as shown in Fig. 7b–d. From the plots, it can be found that there are two regions with remarkably strong nonequilibrium. The first one is still the near-surface region, where ballistic effect dominates. The other one is located within the material and keeps shifting inward with time. Close observation shows that the location of the peak R value is the same as that of the temperature peak (Fig. 6), which indicates that the severe nonequilibrium gives rise to the thermal wave.

4.4. The speed of thermal wave

According to Eq. (4), the speed of the thermal wave is readily obtained as

$$v_T = \sqrt{\frac{\alpha}{\tau}} = \sqrt{\frac{vl}{3\tau}} = \frac{v}{\sqrt{3}}. \tag{21}$$

However, previous research pointed out that the thermal wave does not necessarily propagate at $v/\sqrt{3}$ [3,19]. In particular, v_T is simply the speed of sound if heat pulses transport ballistically. In our simulation results, v_T can be calculated from the distance the peak of the thermal wave travels during a given time interval,

$$v_T = \frac{\Delta x}{\Delta t}. \tag{22}$$

Fig. 8 plots the location of the temperature peaks at different times for femtosecond laser heating discussed in the preceding section. The slope of each straight line corresponds to the calculated speed of the thermal wave. The v_T predicted by the HHCE agrees with Eq. (21), whereas the value from the LBM is equal to the speed of sound v. The results of the HHCE and the LBM differ by a factor of $1/\sqrt{3}$. In the theory of the HHCE, the temperature at any point is defined in sense of thermal equilibrium just as in the PHCE. In other words, it automatically assumes that the thermal energy is distributed over all the directions uniformly. Thus, although phonons travel at the sound speed, thermal pulses travel at a collective speed averaged over all directions [6]. In the diffusive limit, which is common in conventional problems, this assumption turns out to be correct. However, in the current case, the energy density in different directions are not identical due to the ballistic effect. In other words, the transport in the thermal propagation direction is dominant over those in other directions. Therefore, the speed of thermal wave in the ballistic limit is equal to the speed of sound [19].

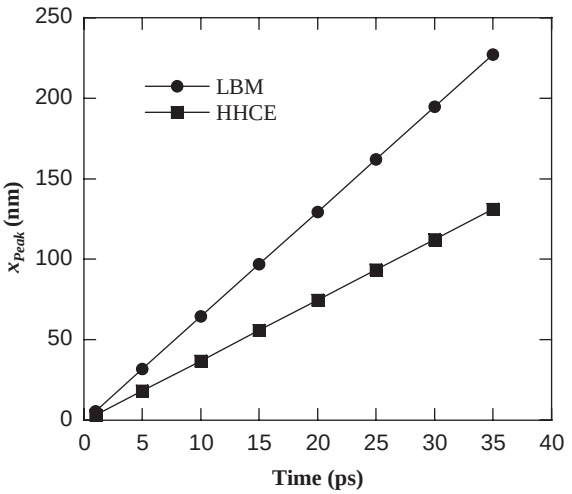

Fig. 8. Location of temperature peak v.s. time.

4.5. Paradox in the heat flux calculation using the HHCE

As shown in previous sections, the PHCE and HHCE failed to predict ballistic transport in very small domains. Regarding the calculation of heat flux, the PHCE uses the Fourier's law

$$\vec{q}'' = -k\nabla T \tag{23}$$

and the HHCE uses Eq. (2), a modified form of Eq. (23). Both of them are based on the idea that the heat flux is proportional to the local temperature gradient. This may not be valid in the cases studied in this work since the continuum concept breaks down in pico- and femto- second laser heating of materials. In this section, the heat flux in the HHCE at time t is calculated by taking the gradient of temperature at time $t-\tau$. On the other

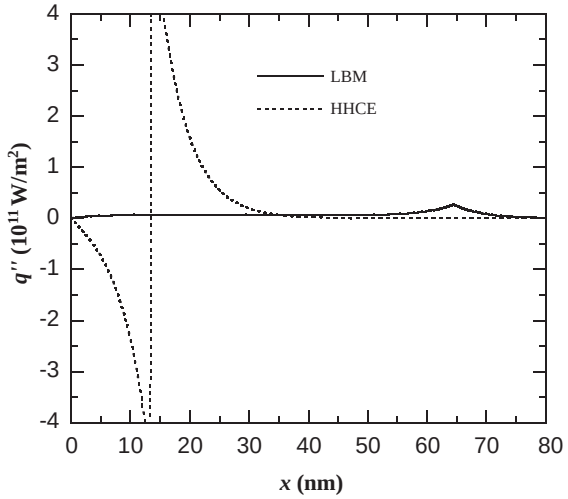

Fig. 9. Spatial distribution of heat flux at 10 ps for femtosecond laser heating.

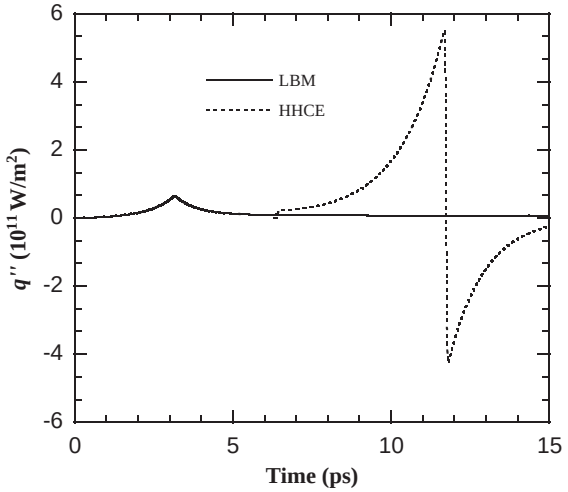

Fig. 10. Time evolution of heat flux at $x = 20$ nm for femtosecond heating.

hand, the heat flux in the LBM is calculated directly using Eq. (13) without resorting to the temperature gradient. Fig. 9 compares the heat flux distributions calculated with these two methods at 10 ps for femtosecond laser heating discussed in Section 4.3. Fig. 10 compares the variation of the heat flux with time at $x = 20$ nm for femtosecond laser heating. In Figs. 9 and 10, it is evident that the heat flux calculated in the HHCE is discontinuous both in time and space. Physically it is unreasonable that without a heating source two immediately neighboring locations have heat fluxes pointing to opposite directions and the heat flux at a location can suddenly be reversed. Moreover, a negative heat flux near the front surface indicates that energy is flowing backward to the heated region. This violates the second law of thermodynamics. While the LBM predicts a much lower heat flux than the HHCE, it does not suffer the above physical discrepancy. From the LBM curves, it can be seen that the heat flux is always positive, indicating a continuous inward energy transfer. The peak of the heat flux can be explained by the presence of the thermal wave. As mentioned in Section 4.3 the thermal wave leads to strong nonequilibrium, which corresponds to an increased difference of energy densities in the positive and negative directions of thermal transport. According to Eq. (13), this strengthened nonequilibrium will lead to a raised heat flux.

5. Conclusion

In this study, the LBM was used to investigate laser heating at time scales from nano- to femtoseconds. The temperature evolutions within a silicon slab exposed to laser pulses were calculated and the results were compared with those of the PHCE and HHCE. It was found that the three methods were equivalent at macroscopic spatial and time limits. For problems involving both short temporal and spatial domains, the thermal transport in the region close to the heated surface was ballistic instead of diffusive. The HHCE, based on the continuum concept, failed to predict this phenomenon. Further investigation of the LBM results showed that the assumption of local equilibrium for the HHCE was questionable because energy flows were severely unbalanced among different directions in the ballistic regime. Due to the dominance of thermal energy in the thermal transport direction, the speed of thermal wave predicted by the LBM was equal to the sound speed in the ballistic limit, rather than $v/\sqrt{3}$

predicted by the HHCE. In addition, the HHCE presumed a proportional relationship between the heat flux and temperature gradient even before equilibrium was established, leading to the discontinuity of the heat flux. The LBM calculated the heat flux directly from microscopic view of energy distribution and did not need equilibrium conditions, so it gave physically reasonable results.

Acknowledgements

This work was supported by the College of Engineering and Technology and the Department of Mechanical Engineering at the University of Nebraska-Lincoln through the faculty start-up fund. Partial support for this work from the National Science Foundation (CTS-0210051) is greatly acknowledged.

References

[1] D.D. Joseph, L. Preziosi, Rev. Mod. Phys. 61 (1989) 41.
[2] D.D. Joseph, L. Preziosi, Rev. Mod. Phys. 62 (1990) 375.
[3] C. Bai, A.S. Lavine, ASME J. Heat Transfer 117 (1995) 256.
[4] C. Körner, H.W. Bergmann, Appl. Phys. A 67 (1998) 397.
[5] A. Majumdar, ASME J. Heat Transfer 115 (1993) 7.
[6] G. Chen, Phys. Rev. Lett. 86 (2001) 2297.
[7] J. Xu, Master Thesis, University of Nebraska-Lincoln, 2004.
[8] F.P. Incropera, D.P. DeWitt, Introduction to Heat Transfer, Wiley, New York, 2000.
[9] C. Cattaneo, Atti del Semin. Mat. e Fis. Univ. 3 (1948) 83.
[10] C.L. Tien, A. Majumdar, F.M. Gerner, Microscale Energy Transport, Taylor and Francis, London, 1998.
[11] P.L. Bhatnagar, E.P. Gross, M. Krook, Phys. Rev. 94 (1954) 511.
[12] S. Hou, Q. Zou, S. Chen, G. Doolen, A.C. Cogley, J. Computat. Phys. 118 (1995) 329.
[13] S.V. Patankar, Numerical Heat Transfer and Fluid Flow, Hemisphere Publishing Corporation, Washington, 1980.
[14] X. Wang, X. Xu, Appl. Phys. A 73 (2001) 107.
[15] D.A. Wolf-Gladrow, Lattice-Gas Cellular Automata and Lattice Boltzmann Models: an introduction, Springer, Netherlands, 1999.
[16] J.Y. Murthy, S.R. Mathur, ASME J. Heat Transfer 124 (2002) 1176.
[17] J.Y. Murthy, S.R. Mathur, ASME J. Heat Transfer 125 (2003) 904.
[18] C. Bai, A.S. Lavine, Heat Transfer Microscale ASME, 253 (1993) 37.
[19] A.A. Joshi, A. Majumdar, J. Appl. Phys. 74 (1993) 31.